Tests of the factorized distorted wave impulse approximation for (p,2p) reactions

C. Samanta
Saha Institute for Nuclear Physics, Calcutta 700 064, India
and Department of Physics and Astronomy, University of Maryland, College Park, Maryland 20742

N. S. Chant, P. G. Roos, A. Nadasen,* and J. Wesick†
Department of Physics and Astronomy, University of Maryland, College Park, Maryland 20742

A. A. Cowley
National Accelerator Centre, Centre for Scientific and Industrial Research, Faure 7131, South Africa
(Received 18 June 1986)

Cross sections for the ^{40}Ca(p,2p) reactions at 101.3 and 76.1 MeV and the ^{16}O(p,2p) reaction at 101.3 MeV have been measured and analyzed using distorted-wave impulse approximation calculations. The sensitivity to the choice of distortion parameters, nonlocality corrections, and spin-orbit terms in the optical potentials have been studied. For the region of phase space studied, the factorization approximation is found to be valid even at energies as low as 76.1 MeV. Extracted spectroscopic factors are compatible with shell model estimates.

I. INTRODUCTION

In recent years, distorted-wave impulse approximation (DWIA) calculations have been used successfully in the analysis of (p,2p) reactions on $1p$ and $2s$-$1d$ shell nuclei. For example, data for the ^{40}Ca(p,2p)^{39}K reaction at 148.2 MeV are in good agreement with factorized DWIA calculations.[1] However, questions have been raised about the validity of the "factorization approximation" for (p,2p) reactions at lower incident energies[2] and, for the ^{16}O(p,2p) reaction, even at proton energies as high as 200 MeV.[3] In the present paper we attempt to study the validity of this approximation and to explore our general understanding of the reaction mechanism at different incident energies such that distortion effects vary in severity. That significant changes in the role of distortion effects occur can be seen in Fig. 1, in which we have calculated the ratios of the DWIA to plane-wave impulse approximation (PWIA) cross sections for the reaction ^{40}Ca(p,2p)^{39}K ($\frac{1}{2}^+$, 2.5 MeV) under kinematic conditions such that, P_3, the recoil momentum of the residual nucleus, is zero. Details of these calculations are discussed in Sec. III. For now we note simply that the calculated ratios falls precipitously as the incident energy is reduced.

Data for the ^{40}Ca(p,2p) reaction at incident energies of 76.1 and 101.3 MeV have been obtained and analyzed together with existing data at 45.0 and 148.2 MeV. In Fig. 1 we note that the ratio of the DWIA to PWIA cross sections is $\sim$0.03 at E_p=76.1 MeV, 0.1 at 101.3 MeV, and 0.21 at 148.2 MeV; i.e., the distortion effects are quite severe at the lower experimental energies. In addition to ^{40}Ca, for which transitions were observed leading to the $2s_{1/2}$ and $1d_{3/2}$ hole states, respectively, we chose to study ^{16}O at an incident energy of 101.3 MeV, for which transitions to $1p_{1/2}$ and $1p_{3/2}$ hole states in ^{15}N dominate the reaction.

In Sec. II, a brief description of the experiment is given. In Sec. III, we describe the DWIA analysis of the data. Further discussion and conclusions are given in Sec. IV.

II. EXPERIMENT

Beams of 76.1 and 101.3 MeV protons from the University of Maryland sector-focused isochronous cyclotron with an energy spread of approximately 150 keV were focused at the center of a 1.5 m diam scattering chamber on a natural calcium target. Gaseous ^{16}O in a cylindrical gas cell of diameter 12.7 cm and depth 6.4 cm

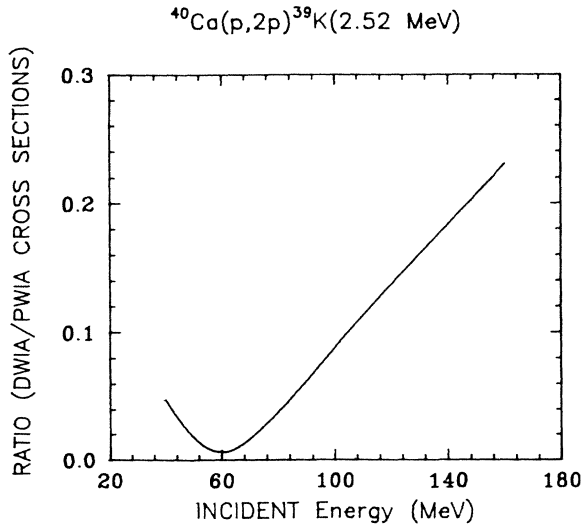

FIG. 1. Ratio of the DWIA to PWIA cross sections vs incident energies for the reaction ^{40}Ca(p,2p)^{39}K (2.52 MeV) at P_3=0 for symmetric quasifree angle pairs.

was used as a second target. The entrance and exit windows of the gas cell were covered with 7.6×10^{-3} mm Havar foil which can withstand a pressure difference of 2 atm. No contamination was found in the gas which could interfere with the observed reactions.

A coincidence experiment was carried out with detector telescopes in a coplanar geometry on both sides of the incident beam. For particle identification, each telescope consisted of one 540 μm thick silicon surface barrier ΔE detector followed by a high purity germanium stopping E detector. One of the germanium E detectors consisted of two crystals. Each detector was equipped with an ion implanted thin front contact to minimize incident particle energy loss and could be recycled from liquid nitrogen to room temperature in order to repair radiation damage. For the gas target, specially designed double-slit collimator systems were used to define the target length and to exclude scattering from the gas cell walls. The overall angular resolution of the two telescopes was 3.1° and 5.0° and the solid angles were 1.9 and 1.6 msr, respectively.

The signals from all the ΔE and E detectors were fed directly to charge sensitive preamplifiers, each of which had both linear and fast timing outputs. All $\Delta E\cdot E$ coincidences were processed using fast electronics such that individual accelerator beam bursts could be resolved. Linear signals, appropriately gated, were digitized and then processed using an on-line IBM 360/44 computer. In addition to signals from the ΔE and E detectors, a time-to-amplitude convertor output, which measured the time difference between the two ΔE signals, permitted simultaneous storage of real and accidental coincidence events. Electronic dead time was measured using a pulser unit, triggered at a rate proportional to beam intensity at the Faraday cup, which provided current signals at each preamplifier input. The data were written on magnetic tapes event by event for subsequent replay.

Data were taken at the angle pairs listed in Table I. With the exception of the 25°/−25° data for ^{16}O(p,2p), these are all quasifree angle pairs so that zero recoil momentum of the residual nucleus is permitted. Data taken at the nonquasifree angle pair might be expected to show some evidence for off-shell effects which become more pronounced at forward angles.[4] Results for both nuclei studied are shown in Fig. 2 as a function of the energy $F3=T1+T2+T3$, where $T1$ and $T2$ are detected particle kinetic energies and $T3$ is the (computed) residual nucleus kinetic energy. Clearly, $F3=T0-B$, where $T0$ is the incident energy and B is the proton-core binding energy. From Fig. 2(a) we see that for the ^{40}Ca(p,2p) reaction two distinct peaks are identified. These correspond to the ground ($\frac{3}{2}^+$) and 2.52 MeV ($\frac{1}{2}^+$) states of ^{39}K and are well resolved. In the ^{16}O(p,2p) spectra, shown in Fig. 2(b) for the angle pair 40.1°/−40.1°, three distinct peaks are identified. The first and third peaks correspond to the ground ($\frac{1}{2}^-$) and 6.32 MeV ($\frac{3}{2}^-$) states of ^{15}N.

In ^{15}N the weak second peak was identified as an unresolved $\frac{5}{2}^+$ (5.27 MeV) and $\frac{1}{2}^+$ (5.299 MeV) doublet. It is interesting to note that these latter states cannot arise from a single-step proton knockout reaction from the p shell. Thus their excitation suggests the existence of 2p-2h components in the structure of ^{16}O or possibly of multistep processes. Further study of these states would be of interest in order to clarify the roles of (2p-2h) components in the ^{16}O target and of multistep transitions via low-lying collective excitations in ^{16}O. Unfortunately, the low statistics prevent detailed study but do suggest the multistep contributions to the $\frac{1}{2}^-$ and $\frac{3}{2}^-$ transitions should

TABLE I. Experimental angle pairs.

Reaction	Incident energy (MeV)	Angle pairs θ_1/θ_2
^{40}Ca(p,2p)^{39}K	76.1	40.0°/−40.0°
		35.0°/−44.5°
		30.0°/−49.0°
		25.0°/−53.0°
		21.0°/−55.0°
^{40}Ca(p,2p)^{39}K	101.3	41.0°/−41.0°
		46.7°/−35.0°
		52.2°/−29.0°
		57.0°/−23.0°
^{16}O(p,2p)^{15}N	101.3	40.1°/−40.1°
		47.0°/−30.0°
		51.0°/−25.0°
		25.0°/−25.0°[a]

[a]Nonquasifree angle pair.

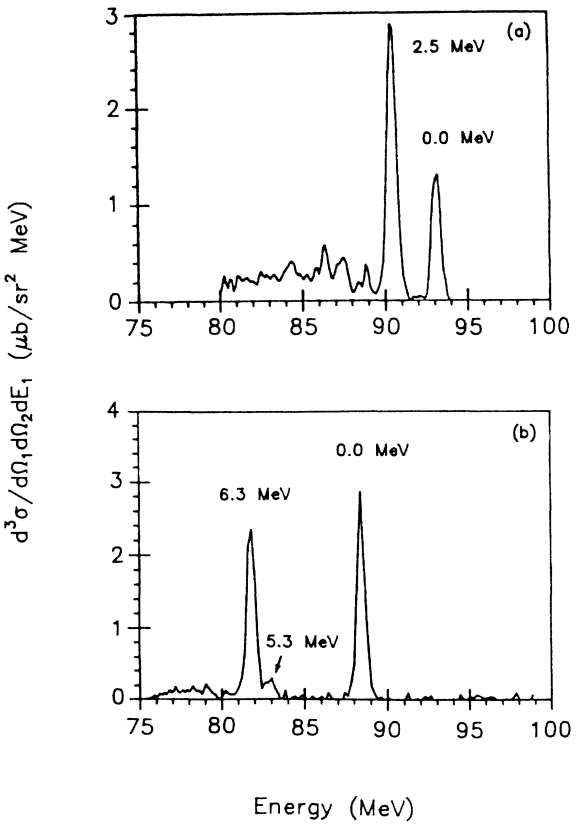

FIG. 2. Binding energy spectra for (a) the ^{40}Ca(p,2p)^{39}K reaction and (b) the ^{16}O(p,2p)^{15}N reaction at 101.3 MeV. The detected proton angles are ±41.0° and ±40.1°, respectively.

not be significant. It is worth noting that, for ^{12}C(p,2p)^{11}B at 50 MeV, a transition to the $\frac{5}{2}^-$ final state at 4.46 MeV, which involves a two-step process, is quite comparable in magnitude to presumably one-step transitions, to other final states.[5] At higher energies[6] the two-step excitation appears to be suppressed. Unfortunately, in the ^{16}O(p,2p)^{15}N experiment at 200 MeV the missing energy resolution was insufficient to resolve these states.[7]

In Figs. 3–5 so called "energy sharing distributions" are shown for the strongly excited residual states. These are differential cross sections for the individual states plotted as a function of the energy of one of the detected protons. The associated theoretical curves are discussed in Sec. III.

III. DWIA ANALYSIS

The data were analyzed using a factorized DWIA in which the cross section for a reaction $A(a,a'b)B$ can be written[8]

$$\frac{d^3\sigma}{d\Omega_{a'}d\Omega_b dE_{a'}} = S_b F_K \frac{d\sigma}{d\Omega_{a-b}} \sum_{\Lambda} |T_L^{\Lambda}|^2 , \tag{1}$$

where S_b is the spectroscopic factor for the bound proton b, F_K is a kinematic factor, and $d\sigma/d\Omega_{a-b}$ is a half-shell two-body cross section for a-b scattering. The quantity $\sum_{\Lambda} |T_L^{\Lambda}|^2$ is a distorted momentum distribution for b in target A, where

$$T_L^{\Lambda} = (2L+1)^{-1/2} \int \chi_{a'}^{(-)*}(\mathbf{r}) \chi_b^{(-)*}(\mathbf{r}) \times \Phi_L^{\Lambda}(\mathbf{r}) \chi_a^{(+)} \left(\frac{B}{A}\mathbf{r} \right) d\mathbf{r} . \tag{2}$$

In Eq. (2) the χ's are distorted waves for the incident and emitted particles and $\Phi_L^{\Lambda}(\mathbf{r})$ is the relative motion wave function for b and B in the target A. In the preceding expressions spin-orbit distortions for the incident and emitted particles are ignored. Nevertheless, owing to the central parts of the optical potentials, for $L \neq 0$ the struck proton, in general, has an effective polarization, P, normal to the scattering plane.[9] Hence, the two-body cross section used in Eq. (1) must be replaced by

$$\frac{d\sigma}{d\Omega} = \left. \frac{d\sigma}{d\Omega} \right|_{\text{unpol}} (1 + PA) , \tag{3}$$

where A is the two-body analyzing power and P is calculable in the DWIA.

If spin-orbit terms are included in the optical potentials, the resultant distorted waves become matrices in spin space $\chi_{\rho\sigma}^{\pm}$ and Eq. (1) has the form[4,10]

$$\frac{d^3\sigma}{d\Omega_{a'}d\Omega_b dE_{a'}} = S_b F_{K'} \sum_{\substack{M \\ \rho_a \rho_{a'} \rho_{b'}}} \left| \sum_{\substack{\Lambda \rho_b \\ \sigma_a \sigma_{a'} \sigma_{b'}}} (L\Lambda \tfrac{1}{2} \rho_b \,|\, JM)(2L+1)^{1/2} T^{L\Lambda}_{\substack{\rho_a \rho_{a'} \rho_{b'} \\ \sigma_a \sigma_{a'} \sigma_{b'}}} \langle \sigma_{a'} \sigma_{b'} \,|\, t \,|\, \sigma_a \rho_b \rangle \right|^2 . \tag{4}$$

Here, $F_{K'}$ is a kinematic factor, ρ_i and σ_i are spin projections for particle i, and b' refers to particle b in the exit channel. In this case the a-b t matrix, although still factored out of the distorted-wave integral, cannot be removed from the coherent sum, and the calculation of the cross section becomes more complicated. Using the above relation, Chant *et al.*[10] found that the effect of including spin-orbit terms in a test of the factorization approximation for the ^{40}Ca(p,2p)^{39}K reaction at $E_p = 148.2$ MeV is small. However, large spin-orbit effects are predicted in some cases.[4,10]

A study of ^{16}O(p,2p)^{15}N at 200 MeV demonstrated[7] the importance of including corrections for the nonlocality of the optical potentials which lead to the well-known[11] damping of the distorted waves in nuclear interior. Estimates were made using effective mass values taken from nuclear matter calculations. In the present analysis these effects are taken into account in a conventional manner by introducing a damping factor $\exp[\beta^2 \mu V(r)/4\hbar^2]$ for each distorted wave, where $V(r)$ is the equivalent local potential, β is the range of nonlocality, and μ is the reduced mass.

In the calculations which follow, using the code, THREEDEE,[4,8,10] values of the two-body t matrix for pp scattering were obtained from an interpolation of available nucleon-nucleon phase shifts.[12] For all cases shown the pp scattering was evaluated at the final proton-proton rest energy (final energy prescription). It has been argued[2] that this choice best approximates the half-shell amplitude, which is the leading term in a Faddeev treatment. The suitability of this approach is demonstrated explicitly in calculations for (p,2p) on ^{7}Li and ^{12}C targets at 100 MeV.[13]

We now describe the results obtained from ^{40}Ca(p,2p) and ^{16}O(p,2p) reactions.

A. The ^{40}Ca(p,2p) reaction

In the DWIA calculations the bound-state parameters were taken from the work of Elton and Swift[14] ($r_0 = 1.3$ fm, $a = 0.6$ fm, $V_s = 12.0$ MeV) and are consistent with elastic electron scattering and with ^{40}Ca(e,ep)^{39}K measurements.[15] For the three scattered waves, we investigated several different optical-potential parameter sets,[16–18] which differed principally in the values of the absorption parameters. Of the parameter sets investigated those obtained by Nadasen *et al.*[16] best match the energy and mass range of our experiment. Use of these parameters yielded the best agreement with the (p,2p) data, and hence were chosen for our final analysis. In the Nadasen parametrization the real potential strength is energy dependent, whereas the imaginary strength does not vary with the energy.

Figures 3 and 4 show the calculated cross sections normalized to the data using the same value of the spectroscopic factor for each state at all scattering geometries studied at a given incident energy. As test cases to examine the effects of spin-orbit potentials and nonlocality, we chose the transitions at the equal angle pairs, where statistical errors are least. Calculations were carried out with and without nonlocality corrections for all three scattered waves ($\beta=0.85$ fm) and with and without spin-orbit terms in the optical potentials for the three scattered waves. The resultant calculations (excluding the no spin-orbit, no nonlocality correction calculation) for the equal angle

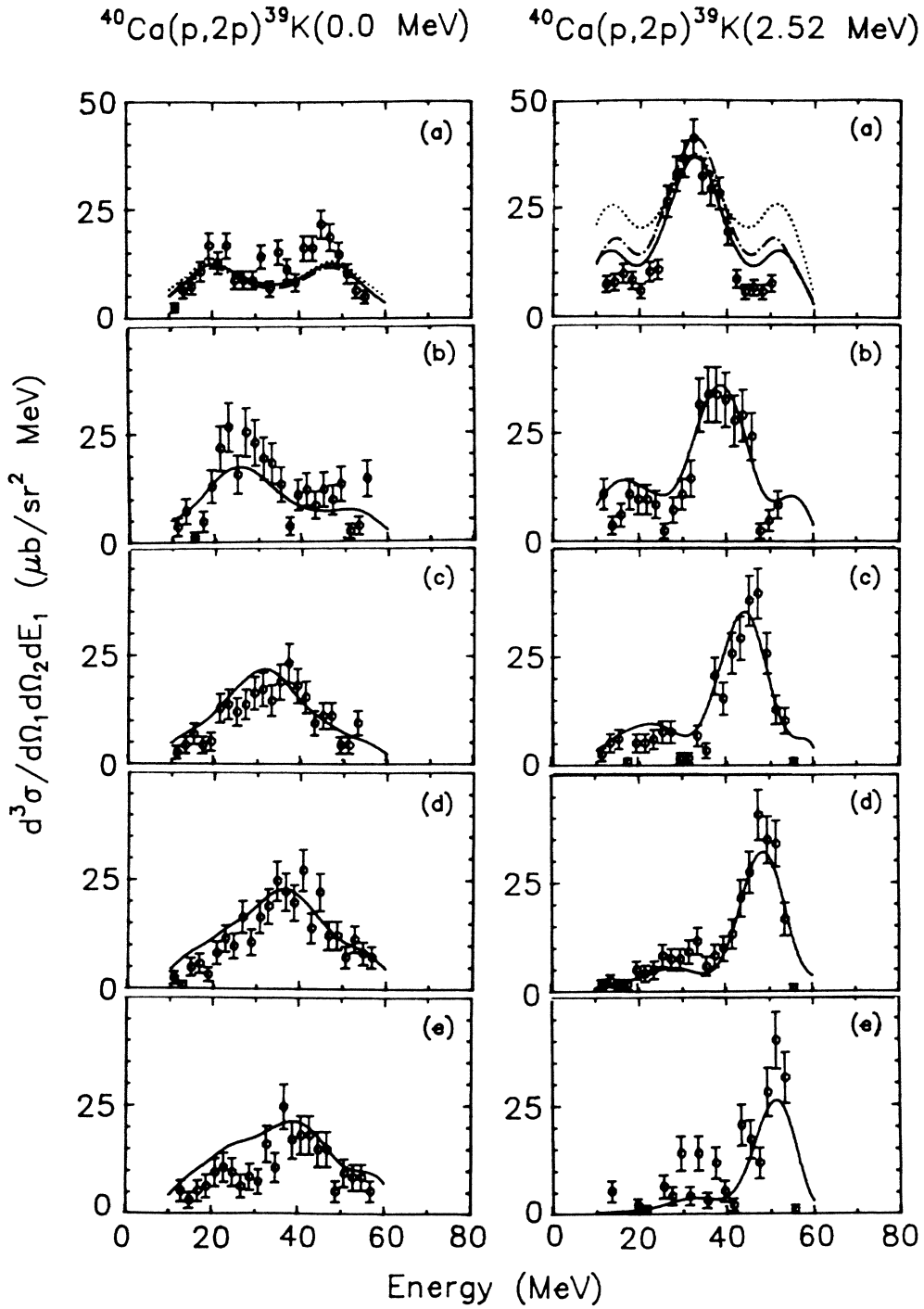

FIG. 3. Energy sharing distributions for ^{40}Ca(p,2p)^{39}K at $E_p=76.1$ MeV at angles (a) 40.0°/−40.0°, (b) 35.0°/−44.5°, (c) 30.0°/−49.0°, (d) 25.0°/−53.0°, and (e) 21.0°/−55.0°. The curves are the results of DWIA calculations: (——), with spin-orbit terms in the optical potentials and nonlocality corrections included for the three scattered waves; · · · ·, with spin-orbit terms, but no nonlocality corrections; —·—·—·, with nonlocality corrections, but no spin-orbit terms. A single spectroscopic factor was used for each state (see Table II).

cases are displayed in Figs. 3(a) and 4(a). All three curves in each panel have the same normalization. One sees that the effects of the spin-orbit potentials are generally small, as expected. The nonlocality corrections for the $\frac{1}{2}^+$ state tend to improve agreement with the data by decreasing the calculated cross sections away from the minimum recoil momentum point. On the whole, for the chosen test cases the calculated cross sections with the Nadasen potential and including nonlocality corrections were found to be in better agreement with the data and hence were used in the calculations for the remaining angle pairs.

In summary, the fits shown in Figs. 3 and 4 are quite good and essentially all of the major features of the data, both detected energy and angular dependence, are reproduced. The calculations for the $L=0$ data ($\frac{1}{2}^+$, 2.52 MeV) have a tendency to be somewhat too broad and many of the DWIA calculations tend to overpredict the cross section for larger values of recoil momentum. This may reflect inadequacies in either the optical-model potentials or the bound-state wave functions. The comparison shown is particularly demanding on the optical model description, requiring potentials which accurately predict distortion effects over a significant range of incident energies.

To emphasize this point we refer again to Fig. 1, in which the ratio of DWIA to PWIA cross section is shown

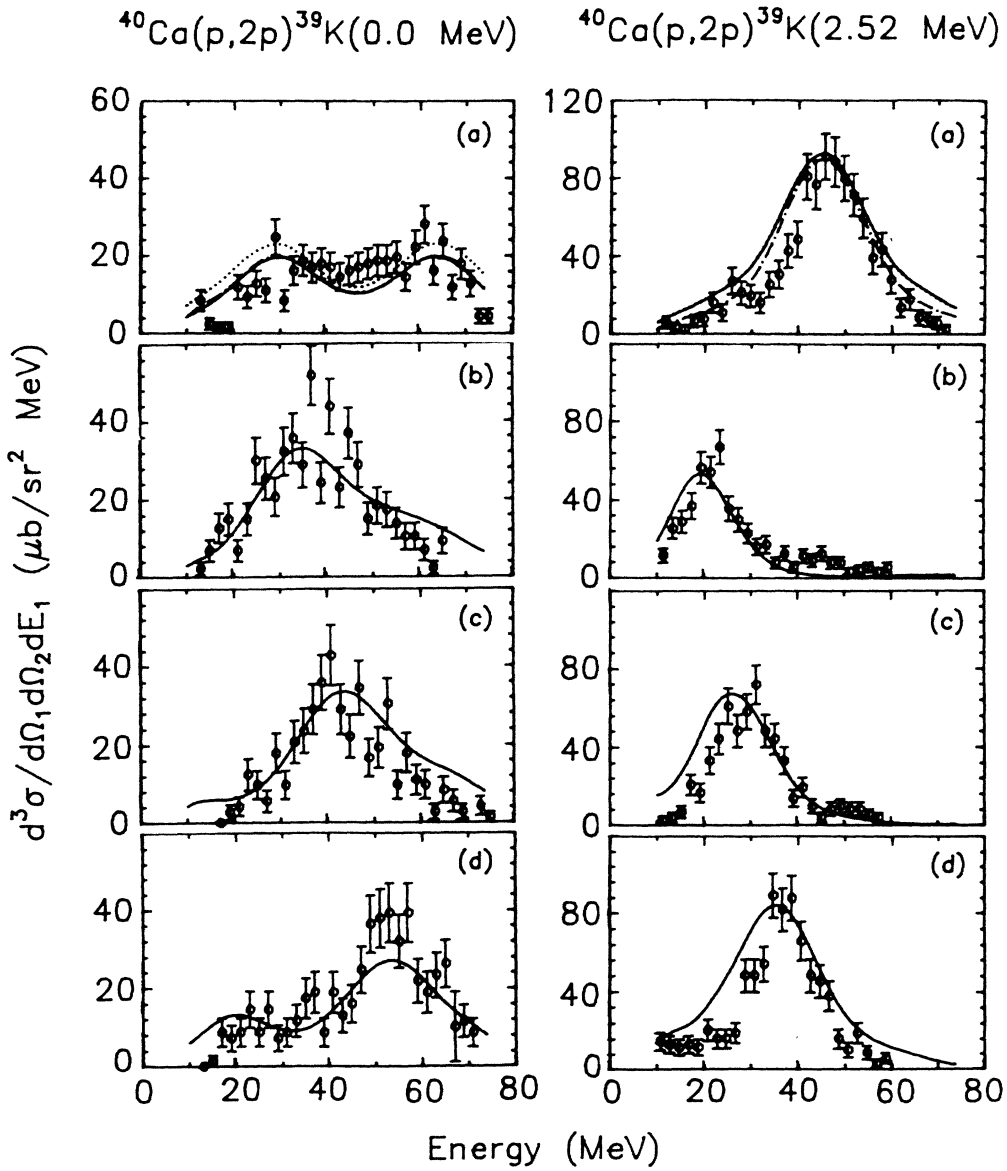

FIG. 4. Energy sharing distributions for ^{40}Ca(p,2p)^{39}K at 101.3 MeV at angles (a) 41.0°/−41.0°, (b) 46.7°/−35.0°, (c) 52.2°/−29.0°, and (d) 57.0°/−23.0°. The curves are the results of DWIA calculations: ——, with spin-orbit terms in the optical potentials and nonlocality corrections included for the three scattered waves; · · · ·, with spin-orbit terms, but no nonlocality corrections; —·—·—·, with nonlocality corrections, but no spin-orbit terms. A single spectroscopic factor was used for each state (see Table II).

for the ^{40}Ca(p,2p)^{39}K (2.52 MeV) transition as a function of incident energy. The calculations employ the Elton-Swift bound state[14] and the scattering potentials of Nadasen *et al.*[16] used for the calculations of Figs. 3 and 4. Nonlocality corrections were included and the emitted particles were assumed to be detected in a coplanar symmetric geometry with equal energies, such that the residual ^{39}K was left at rest. It is seen that the predicted reduction in cross section due to the distorting potentials is only $\sim$0.25 at 150 MeV, but becomes almost an order of magnitude more severe as the incident energy is reduced. In view of such changes the generally good agreement in shape between the data of Figs. 3 and 4 and the DWIA predictions is encouraging. Nevertheless, the results of Fig. 1 suggest the importance of a comparison between predicted and observed *absolute* cross sections. We shall return to this issue in Sec. IV.

B. The ^{16}O(p,2p)^{15}N reaction

For the ^{16}O(p,2p)^{15}N reaction we again took the bound-state potential parametrization from the work of Elton and Swift[14] ($r_0=1.41$ fm, $a=0.65$ fm, $V_s=13.0$ MeV). Unfortunately, in this mass and energy range no global optical-model analysis exists. Since we believe that the mass and energy systematics are most important in DWIA calculations of this type, we decided to utilize the potential of Nadasen *et al.*[16] Despite the extrapolation beyond the mass range of the elastic scattering data used in the analysis, the resultant fits to the data were found to be generally good for the quasifree angle pairs. These are shown in Fig. 5, again with a single normalization for each state. Calculations were also carried out with other optical-model potentials which fit elastic scattering data at a single energy.[19–22] Generally, these fits to the shape were somewhat poorer and the spectroscopic factors in poorer agreement with other types of measurements.

As in the case of ^{40}Ca(p,2p), calculations were carried out to examine the effects of spin-orbit terms in the optical potentials and nonlocality corrections. These are shown in Fig. 5(a) for the equal angle case. For ^{16}O the effects, although generally larger than for ^{40}Ca, are quite small. The inclusion of nonlocality corrections gives rise to about a 20% reduction in cross section, whereas inclusion of spin-orbit terms in the optical potentials for the scattered waves increases the cross section by approximately 10%. The remainder of the calculations were carried out including spin-orbit terms and nonlocality corrections. Overall, as for ^{40}Ca(p,2p) the fits to the quasifree angle pairs are very good, and, as discussed in Sec. IV, lead to a spectroscopic factor of reasonable magnitude.

At the forward nonquasifree angle pair [Fig. 5(d), 25.0°/$-$25.0°] the calculated energy-sharing distribution using the final-energy prescription (FEP) agrees rather well with the data in terms of magnitude. However, the calculated distributions are rather flat. In contrast, at least for the 6.3 MeV level, the experimental data suggest a double-humped structure. At these more forward angles differences between the on-shell p-p cross section, using both the FEP and the IEP (initial-energy prescription), and the half-shell cross section become more pronounced. However, the relatively good agreement in magnitude indicates that, on the average, such effects are not yet severe at this angle pair. The disagreement in shape may indicate the onset of more detailed off-shell effects or the beginnings of a breakdown in the factorized DWIA theory. For ^{12}C(p,2p)^{11}B at 100 MeV, fairly significant discrepancies are noted between experiment and factorized DWIA calculations using half-shell t matrices calculated from the Reid soft-core potential.[13] Nonfactorized calculations[23] using a rather crude t matrix do predict a flattening of the coplanar symmetric angular correlation in agreement with experiment. Whether the opposite behavior would be predicted for the energy sharing distribution has not been established. However, it does seem unlikely.

IV. DISCUSSION

In the preceding section we have shown that the DWIA calculations fit the shape of the experimental data quite well. Next, we evaluate the validity of the factorization approximation made in our DWIA analysis; finally, we discuss the extracted spectroscopic factors relating the absolute magnitudes of the experimental and theoretical cross sections.

A. Validity of the factorization approximation

In the approximation that spin-orbit distortions can be ignored we may construct the quantity

$$Q(\theta_1,\theta_2)=\frac{d^3\sigma(\theta_1,\theta_2)}{d\Omega_{a'}d\Omega_b dE_{a'}}\left[F_K\sum_{\Lambda}|T_L^{\Lambda}|^2\right]^{-1}, \tag{5}$$

where

$$\frac{d^3\sigma(\theta_1,\theta_2)}{d\Omega_{a'}d\Omega_b dE_{a'}}$$

is the experimental three-body cross section at the laboratory angle pair (θ_1,θ_2) for the $A(a,a',b)B$ reaction. If the factorization approximation is satisfactory, we obtain

$$Q(\theta_1,\theta_2)=S_b\frac{d\sigma}{d\Omega_{a-b}}, \tag{6}$$

i.e., Q should be identical to the two-body cross section to within normalization by the spectroscopic factor. The inclusion of spin-orbit distortions formally destroys the factorization in cross section,[10] although the amplitudes are still taken as a product of distorted wave and two-body terms. In practice, as indicated in each panel (a) of Figs. 3–5, the corrections at the kinematic points considered here are quite small. Thus, the success or failure of the physical approximation is best displayed in the form given in Eq. (6), with an additional correction factor f showing the effects of spin-dependent distortions. In the analysis which follows the derived quantity Q is compared both with the two-body cross section $d\sigma/d\Omega$ and with $f(d\sigma/d\Omega)$, in which spin-orbit effects are properly included. Note that the two-body cross section $d\sigma/d\Omega$ for an $L\neq 0$ case is that for a polarized target nucleon as indicated in Eq. (3).

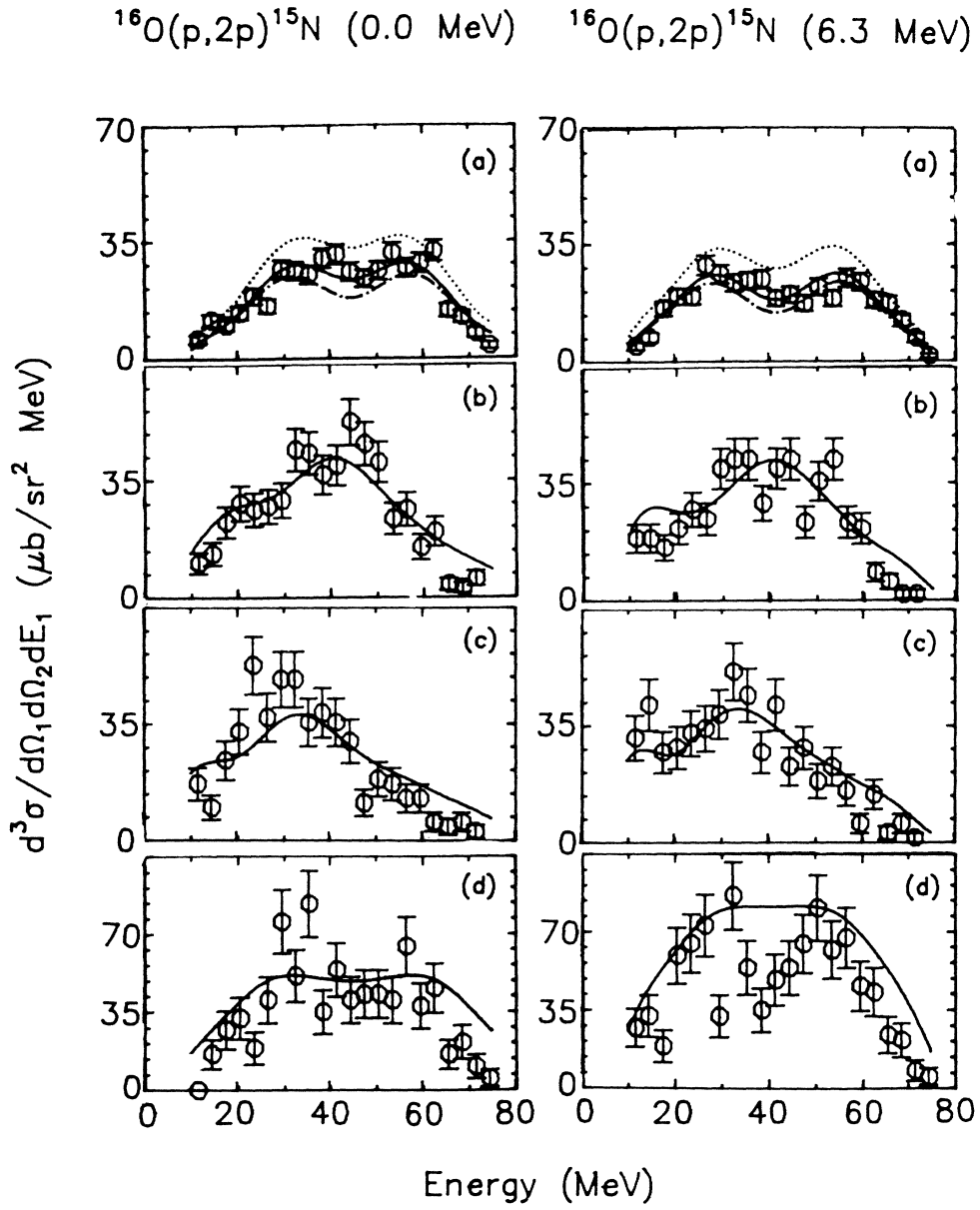

FIG. 5. Energy sharing distributions for ^{16}O(p,2p)^{15}N at $E_p = 101.3$ MeV at angles (a) 40.1°/−40.1°, (b) 47.0°/−30.0°, (c) 51.0°/−25.0°, and (d) 25.0°/−25.0°. The curves are the results of DWIA calculations: ——, with spin-orbit terms in the optical potentials and with nonlocality corrections included for the three scattered waves; · · · ·, with spin-orbit terms, but no nonlocality corrections; —·—·—·, with nonlocality corrections, but no spin-orbit terms. A single spectroscopic factor was used for each state (see Table II).

Using the data at the quasifree angle pairs, we have performed a factorization test for the $L = 0$ and 2 transitions observed for the ^{40}Ca(p,2p)^{39}K reaction and for the ^{16}O(p,2p)^{15}N, $L = 1$ transitions. The data points shown in Figs. 6–8 represent the right-hand side of Eq. (5) using our cross sections measured at the $P_3 \approx 0$ point for the $L = 0$ transition, and at the peaks in the energy sharing spectra for the $L \neq 0$ transitions. In each case the quantity Q has been arbitrarily scaled to optimize agreement with the magnitude of the two-body data. In Figs. 6–8 we see that within experimental errors the approximation is found to be valid for the ^{40}Ca target at $E_p = 76.1$ and 101.3 MeV and for the ^{16}O target at $E_p = 101.3$ MeV.

This result is somewhat surprising since at these energies the two-body p-p cross sections vary significantly with relative momentum. Thus, one might expect momentum spreading caused by distortion to destroy the factorization. However, the result may, in part, be due to changes in radial localization of the (p,2p) reaction with energy. We have calculated the contributions to the cross sections for the ^{40}Ca(p,2p) (2.5 MeV, $L = 0$ transition) reaction at the $P_3 = 0$ point from different radial zones of the nucleus. This calculation is carried out by introducing a lower radial cutoff into the calculation of the amplitude

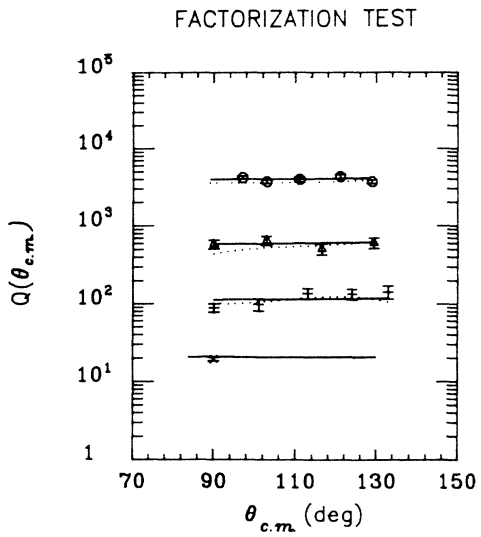

FIG. 6. Test of the factorization approximation: ^{40}Ca(p,2p)^{39}K (2.52 MeV) at (from top to bottom) $E_p = 148.2$ MeV ($\times 10^3$), ⊖; 101.3 MeV ($\times 10^2$), ⧓; 76.1 MeV ($\times 10^1$), ⧖; and 45.0 MeV ($\times 10^0$), ⋈. The curves are the two-body unpolarized cross section σ_{pp} (——) and $f\sigma_{pp}$ (· · · ·), where f is a correction due to the spin-orbit potentials.

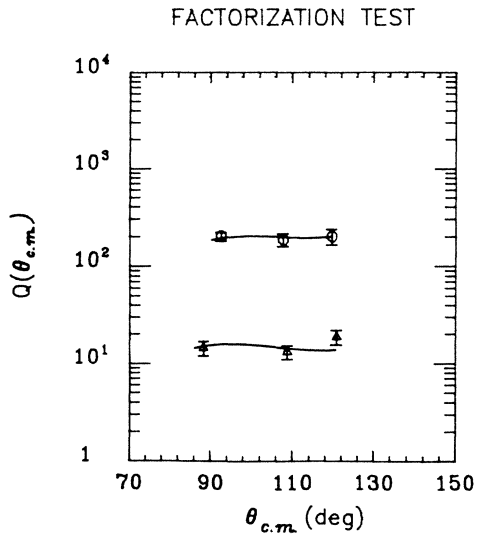

FIG. 8. Test of the factorization approximation: ^{16}O(p,2p)^{15}N at 101.3 MeV for (from top to bottom) the excited state (6.32 MeV) ($\times 10^1$), ⊖, and the ground state (0.0 MeV) ($\times 10^0$), ⧓. The solid curve is the two-body cross section for a polarized nucleon $\sigma_{pp}(1+PA)$, where P is the effective polarization of the target nucleon predicted by the DWIA and A the nucleon-nucleon analyzing power.

T_L^{Δ} of Eq. (2). Differential cross sections are then computed for a series of cutoff radii increasing from zero in 0.5 fm steps. Differences between calculations for adjacent cutoff radii then yield the histogram shown in Fig. 9. In this figure we see that as the incident energy decreases the $L=0$ transition in ^{40}Ca(p,2p) becomes more and more surface localized and, at $P_3=0$, where we have studied the factorization approximation, the contributions to the cross sections come mostly from the tail of the bound-state wave function. Consequently, due to greater surface localization of the reaction at low incident energies, the spread of momenta remains small enough so that the factorization approximation is not destroyed. Similar behavior is to be expected for the $L=1$ and 2 transitions studied.

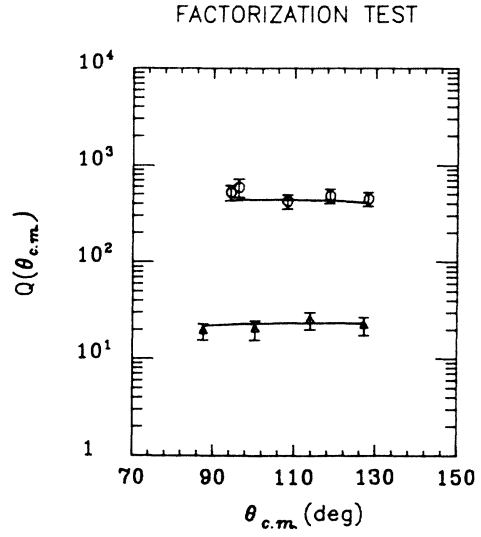

FIG. 7. Test of the factorization approximation: ^{40}Ca(p,2p)^{39}K (0.0 MeV) at $E_p =$ (from top to bottom) 101.3 MeV ($\times 10^1$), ⊖; and 76.7 MeV ($\times 10^0$), ⧓. The solid curve is the two-body cross section for a polarized struck nucleon $\sigma_{pp}(1+PA)$, where P is the effective polarization of the target nucleon predicted by the DWIA and A the nucleon-nucleon analyzing power.

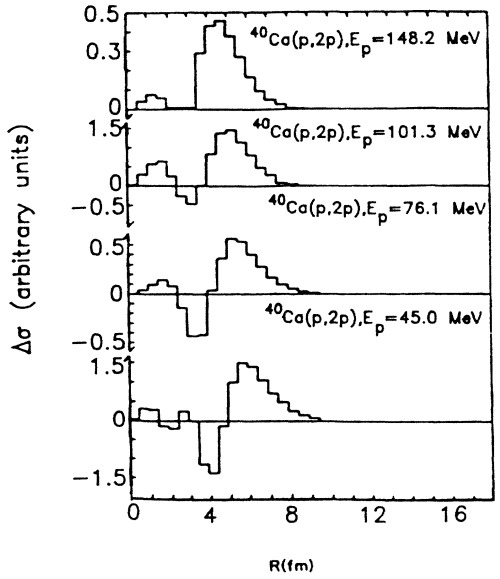

FIG. 9. Radial localization of the contribution to the DWIA cross section at various incident energies for the ($\frac{1}{2}^+$, 2.52 MeV) state of ^{39}K at $P_3=0$.

TABLE II. Spectroscopic factors.

Levels ^{39}K	Incident energy	^{40}Ca(p,2p)^{39}K[a] Energy sharing Figs. 3–4	Factorization Figs. 6–7	(e,ep)[b]	(d,^{3}He)	(τ,α)[c]
$\frac{1}{2}^+$, 2.52 MeV	148.2		1.0	1.3	1.65[c]	1.6
($L=0$)	101.3	1.0	1.1		1.62[d]	
	76.1	1.3	1.5			
	45.0		1.0			
$\frac{3}{2}^+$, 0.00 MeV	101.3	4.2	3.9		3.70[c]	4.3
($L=2$)	76.1	5.0	6.0		4.23[d]	

Levels ^{15}N	Incident energy	^{16}O(p,2p)^{15}N[a] Energy sharing Fig. 5	Factorization Fig. 8	(p,2p)[f]	(d,^{3}He)[g]	(p,d)
$\frac{1}{2}^-$, 0.00 MeV	101.3	2.15	2.15	1.4	2.1	2.4[h]
($L=1$)						2.0[i]
$\frac{3}{2}^-$, 6.32 MeV	101.3	3.1	3.1	2.8	3.7	3.4[h]
($L=1$)						3.5[i]

[a]Present analysis.
[b]Reference 15.
[c]Reference 25.
[d]Reference 26.
[e]Analog transition, Ref. 27.
[f]Reference 3.
[g]Reference 26.
[h]Analog transition, Ref. 28.
[i]Analog transition, Ref. 29.

We have also reanalyzed the previously published data[1] for the ^{40}Ca(p,2p) reaction at 148.2 MeV and[24] at $E_p=45$ MeV. The 148.2 MeV results are shown in Fig. 6, and as previously indicated, support the factorization approximation. For the data at 45 MeV we could not perform a conventional test of the factorization approximation since data exist at only one quasifree angle pair. However, as discussed below, for that one data point we find that even at this low incident energy our DWIA analysis predicts a spectroscopic factor comparable to that at the other energies.

B. Extraction of the spectroscopic factors

The spectroscopic factors extracted from normalization of the DWIA calculations to the experimental data are presented in Table II. Results are presented both for the normalization selected for the energy sharing distributions shown in Figs. 3–5 and for the angular distributions constituting the factorization tests shown in Figs. 6–8. Since different subsets of the data are involved in two cases, these two sets of spectroscopic factors differ somewhat ($<20\%$).

With the use of the optical-model parameters of Ref. 16 throughout, we obtain reasonably consistent spectroscopic factors at all energies for ^{40}Ca(p,2p)^{39}K. It should be noted that our reanalysis of the 148.2 MeV data yields $C^2S=1.0$, in contrast to the published value of 1.4 obtained with a different optical-model parameter set. For both the $L=0$ and 2 transitions, the spectroscopic factors at 76 MeV are roughly 25% larger than at the other energies. Discrepancies of this size may well originate from the optical-model potential description. We note that the extracted $d_{3/2}$ spectroscopic factor is close to the expected closed-shell value of 4.0. However, the $2s_{1/2}$ value is considerably smaller than the expected value of 2.0.

The values for ^{40}Ca(p,2p)^{39}K are also in fair agreement with the values obtained from other reactions as indicated in Table II. Overall, the agreement in spectroscopic factors for different bombarding energies and for different reactions is satisfactory, considering the uncertainties in any distorted-wave analysis, and thus supports the use of a DWIA analysis.

For ^{16}O(p,2p)^{15}N we obtain quite reasonable values of $C^2S=2.15$ for the ground state ($\frac{1}{2}^-$), compared to the closed-shell limit of 2.0, and $C^2S=3.1$ for the excited state ($\frac{3}{2}^-$), compared to the closed shell limit of 4.0. These are in line with both expectations (part of the $\frac{3}{2}^-$ strength lies at 10 MeV excitation) and other measurements (see Table II). One disagreement with previous work is that with the 200 MeV ^{16}O(p,2p) analysis in which the spectroscopic factor for the ground state is only about $\frac{1}{2}$ of our present value. In addition, the ratio of $\frac{3}{2}^-$ to $\frac{1}{2}^-$ is 2.0 at 200 MeV compared to our present ratio of 1.45. Part of this ratio discrepancy may be due to inclusion of additional $\frac{3}{2}^-$ strength at 10 MeV in the poorer energy resolution, 200 MeV results. However, the major difficulties probably arise from the need for a more consistent optical-model parameter set for these light nuclei.

V. CONCLUSIONS

In summary, we have obtained fairly consistent values of the spectroscopic factors for the (p,2p) reactions using the DWIA theory. We find that the factorization approx-

imation works even when distortion effects are quite severe. However, we note that, for the kinematic regions studied, the reaction is fairly surface localized. Indeed, a problem remains for the forward angle data for which the off-shell effects are potentially large and for which contributions to the reaction from the nuclear interior are more significant.

For the factorization approximation to be successful it is necessary that changes in the momenta of the incident and emitted particles from the asymptotic values be small enough that the corresponding two-body t matrix can be computed for the asymptotic kinematics. This can occur if the distorting potentials are sufficiently weak or if distortions result simply in a multiplicative attenuation factor.[30] As an alternative, strong distortion effects can conspire to produce, through both attenuation and phasing effects, strong surface localization. In this case the requirements for factorization can be met in the limited surface region yielding significant contributions to the differential cross section. This appears to be the case for much of the present data. It is also interesting to note that this same behavior is found for the $(\alpha,2\alpha)$ reaction[31] at 140 MeV incident energy, in which factorization appears to work over roughly 2 orders of magnitude variation in the two-body cross section. The factorization approximation is also quite successful for the ^{9}Be$(\vec{p},p\alpha)^{5}$He reaction[32] at 150 MeV. Clearly, additional theoretical and experimental studies of this issue are of interest.

This work was supported in part by the U.S. National Science Foundation.

---

*Present address: Department of Natural Sciences, University of Michigan—Dearborn, Dearborn, MI 48128.

†Present address: TRIUMF, Vancouver, British Columbia, Canada V6T 2A3.

[1]P. G. Roos, N. S. Chant, D. W. Devins, D. L. Friesel, W. P. Jones, A. C. Attard, R. S. Henderson, I. D. Svalbe, B. M. Spicer, V. C. Officer, and G. G. Shute, Phys. Rev. Lett. **40**, 1439 (1978).

[2]Edward F. Redish, G. J. Stephenson, Jr., and Gerald M. Lerner, Phys. Rev. C **2**, 1665 (1970).

[3]P. Kitching, C. A. Miller, D. A. Hutcheon, A. N. James, W. J. McDonald, J. M. Cameron, W. C. Olsen, and G. Roy, Phys. Rev. Lett. **37**, 1600 (1976).

[4]N. S. Chant, in *The Interaction Between Medium Energy Nucleons in Nuclei—1982, IUCF,* AIP Conf. Proc. No. 97, edited by H. O. Meyer (AIP, New York, 1983), p. 205.

[5]H. G. Pugh, D. L. Hendrie, Marc Chabre, and E. Boschitz, Phys. Rev. **155**, 1054 (1967).

[6]D. W. Devins, D. L. Friesel, W. P. Jones, I. D. Svalbe, B. M. Spicer, V. C. Officer, G. G. Shute, and R. S. Henderson, Aust. J. Phys. **32**, 323 (1979).

[7]P. Kitching, C. A. Miller, W. C. Olsen, D. A. Hutcheon, W. J. McDonald, and A. W. Stetz, Nucl. Phys. **A340**, 423 (1980).

[8]N. S. Chant and P. G. Roos, Phys. Rev. C **15**, 57 (1977).

[9]G. Jacob, Th. A. J. Maris, C. Scheider, and M. R. Teodoro, Phys. Lett. **45B**, 181 (1973); Gerhard Jacob, Th. A. J. Maris, C. Scheider, and M. R. Teodoro, Nucl. Phys. **A257**, 517 (1976).

[10]N. S. Chant, P. Kitching, P. G. Roos, and L. Antonuk, Phys. Rev. Lett. **43**, 495 (1979); N. S. Chant and P. G. Roos, Phys. Rev. C **27**, 1060 (1983).

[11]F. Perey and B. Buck, Nucl. Phys. **32**, 353 (1962).

[12]C. A. Miller, private communication.

[13]R. K. Bhowmik, C. C. Chang, J.-P. Didelez, and H. D. Holmgren, Phys. Rev. C **13**, 2105 (1976).

[14]L. R. B. Elton and A. Swift, Nucl. Phys. **A94**, 52 (1967).

[15]J. Mougey, M. Bernheim, A. Bussiere, A. Gillebert, Phan Xuan Hô, M. Priou, D. Royer, I. Sick, and G. J. Wagner, Nucl. Phys. **A262**, 461 (1976).

[16]A. Nadasen, P. Schwandt, P. P. Singh, W. W. Jacobs, A. D. Bacher, P. T. Debevec, M. D. Kaitchuck, and J. T. Meek, Phys. Rev. C **23**, 1023 (1981).

[17]W. T. H. Van Oers, Phys. Rev. C **3**, 1550 (1971).

[18]F. D. Becchetti and G. W. Greenless, Phys. Rev. **182**, 1190 (1969).

[19]Gerald M. Lerner and J. B. Marion, Nucl. Phys. **A193**, 593 (1972).

[20]T. Y. Li and S. K. Mark, Can. J. Phys. **46**, 2645 (1968).

[21]R. N. Boyd, J. C. Lombardi, R. Mohan, R. Arking, and A. B. Robbins, Nucl. Phys. **A182**, 571 (1972).

[22]J. A. Fannon, E. J. Burge, D. A. Smith, and N. K. Ganguly, Nucl. Phys. **A97**, 263 (1967).

[23]K. L. Lim and I. E. McCarthy, Nucl. Phys. **88**, 433 (1966).

[24]K. H. Bray, S. N. Bunker, M. Jain, K. S. Jayaraman, C. A. Miller, J. M. Nelson, W. T. H. Van Oers, D. O. Wells, J. Janiszewski, and I. E. McCarthy, Phys. Lett. **35B**, 41 (1971).

[25]P. Doll, G. J. Wagner, K. T. Knöpfle, and G. Mairle, Nucl. Phys. **A263**, 210 (1976).

[26]J. C. Hiebert, E. Newman, and R. H. Bassel, Phys. Rev. **154**, 898 (1967).

[27]R. Bock, H. H. Duhm, and R. Stock, Phys. Lett. **18**, 61 (1965).

[28]P. G. Roos, S. M. Smith, V. K. C. Cheng, G. Tibell, A. A. Cowley, and R. A. J. Riddle, Nucl. Phys. **A255**, 187 (1975).

[29]J. Källne, Gustaf Werner Institut Report No. GWI-PH 2/74, 1974 (unpublished).

[30]See, for example, Th. A. J. Maris, in *Nuclear and Particle Physics at Intermediate Energies (1976),* edited by J. B. Warren (Plenum, New York, 1976), p. 425.

[31]C. W. Wang, N. S. Chant, P. G. Roos, A. Nadasen, and T. A. Carey, Phys. Rev. C **21**, 1705 (1980).

[32]C. W. Wang, P. G. Roos, N. S. Chant, G. Ciangaru, F. Khazaie, and D. J. Mack, Phys. Rev. C **31**, 1662 (1985).